

Deep Neural Networks Fused with Textures for Image Classification

Asish Bera^{1*}, Debotosh Bhattacharjee² and Mita Nasipuri²

¹*Department of Computer Science and Information Systems, BITS Pilani, Rajasthan, India.

²Department of Computer Science and Engineering, Jadavpur University, Kolkata, WB, India.

*Corresponding author(s). E-mail(s): asish.bera@pilani.bits-pilani.ac.in;

Abstract

Fine-grained image classification (FGIC) is a challenging task in computer vision for due to small visual differences among inter-subcategories, but, large intra-class variations. Deep learning methods have achieved remarkable success in solving FGIC. In this paper, we propose a fusion approach to address FGIC by combining global texture with local patch-based information. The first pipeline extracts deep features from various fixed-size non-overlapping patches and encodes features by sequential modeling using the long short-term memory (LSTM). Another path computes image-level textures at multiple scales using the local binary patterns (LBP). The advantages of both streams are integrated to represent an efficient feature vector for image classification. The method is tested on eight datasets representing the human faces, skin lesions, food dishes, marine lives, etc. using four standard backbone CNNs. Our method has attained better classification accuracy over existing methods with notable margins.

Keywords: Convolutional Neural Networks; Face Recognition; Food Classification; Hand Shape; Local Binary Patterns; Marine Life; Palmprint; Random Erasing Data Augmentation; Skin Lesions.

1 Introduction

Fine-grained image classification (FGIC) is a challenging problem in computer vision since the past decades [1]. It discriminates smaller visual variations among various sub-categories of objects like human faces, flowers, foods, etc. The convolutional neural networks (CNNs) have achieved high performance in FGIC. The CNNs represent object's shape, texture, and

other correlated information in the feature space. In addition with global image-level description, object-parts relation, and local patch information have shown their efficacy by mining finer details to solve FGIC. Many works have been devised leveraging attention mechanism [2], [3]; context encoding [4], [5]; erasing data augmentation [6], [7], and others. Many works avoid bounding-box annotations to localize essential image-regions using weakly supervised part selection [8]. Thus, defining region-based descriptors is a key aspect to enhance FGIC performance.

In another direction, the local binary patterns (LBP) [9] have achieved significant success in describing textural features from human faces, and other image categories [10]. LBP is a non-parametric texture descriptor, extracted from a grayscale image. It encodes the differences between a pixel and its neighborhood pixels localized in a rectangular grid *e.g.*, 3×3 , etc. Here, both the textural and deep features are fused to formulate an efficient feature vector for image classification. This work proposes a method namely, Deep (Neural) Networks fused with Textures (DNT) to explore its aptness for FGIC. The first path extracts deep feature map using a base CNN. Then, the high-level deep feature maps is pooled through a set of non-overlapping patches. Next, a global average pooling (GAP) layer is applied to summarize the features followed by patch-encoding using the long short-term memory (LSTM). The other path computes the histograms of LBPs as local texture-based feature descriptors. Finally, these two sets of features are mixed prior to a classification layer. We have experimented on eight small-scale image datasets (1k-15k), representing a wide variations in the object’s shape, color, background, texture, etc. The datasets includes human faces with age-variations [11], [12]; hand shapes/palmpoint [13], skin lesions [14], natural objects like flowers, underwater sea-lives; and food-dishes of India [15] and Thailand [16]. This paper is an improvement of our earlier published work [17]. Currently, this extended work contains new results tested on two more datasets representing hand-shape and skin lesions, including the results of previous work. The contributions of this paper are as follows:

- The deep features and local binary patterns are fused for image recognition.
- The method achieves satisfactory accuracy on eight image datasets representing the human faces, hand, skin lesions, food dishes, and natural object categories.

The rest of this paper is organized as follows: Section 2 summarizes related works, and Section 3 describes the proposed method. The experimental results are discussed in Section 4, followed by the conclusion in Section 5.

2 Related Works

Human faces, food items, and other objects (*e.g.*, flowers, marine lives, etc.) recognition is a challenging FGIC task. Apart from global feature descriptor rendered from a full-image, patch-descriptors have attained remarkable progress using deep learning. Part-based methods focusing on local descriptions and semantic correlations are integrated [3]. In this direction, multi-scale region proposals, and fixed-size patches have attained much research attention. In [5], multi-scale region features are encoded via the LSTM units. In [4], mask-RCNN is employed to localize discriminative regions. Several approaches have explored attention mechanism to improve FGIC performance including food recognition [3]. Few methods have proposed an ensemble of various CNNs, fusion of two or more sub-networks for performance

gain [15]. Recently, vision transformers (ViT) have embedded non-overlapping patches with multi-head self-attention module [18]. The performance can be boosted by the random erasing data augmentation for multi-scale patch-based feature representation [7]. Various food-dishes classification is discussed in [19], [20], [21]. Researchers have summarized a comprehensive study on FGIC [1], and food recognition [22]. The Forward Step-wise Uncertainty-Aware Model Selection has described an deep learning based ensemble method for food-dishes classification [23]. Underwater object detection, segmentation, and classification is a challenging research area in computer vision. Studies on the marine lives detection using deep learning techniques are summarized in [24], [25]. Also, early diagnosis of skin cancer from skin lesions using hybrid models CNN-ANN and CNN-RF is presented [14]. A survey in this direction has been studied in [26]. Several benchmark public datasets are developed by the International Skin Imaging Collaboration (ISIC) for detection and classification of skin cancer, melanoma, and lesions using dermoscopy images [27], [28], [29]. Marine-life classification using transfer learning based on pre-trained CNNs is described [30]. A video dataset on underwater marine animals of six categories is proposed with baseline results [31].

Before the deep learning era, different local shape and texture information including the LBP, geometric properties, shape profiles, bag of words, Scale Invariant Feature Transform (SIFT), colors, and many more have been described in the literature [32], [33], [13], [34], [26], [14], [35], [36]. Most of these conventional feature descriptors are used for recognizing the human faces, emotions, hand-shape, palmprint, skin lesions, and other biometric modality and object categories. A significant number of works on face recognition have computed local textures using the LBP family and others. A classical gray-scale, rotation invariant, and uniform LBP at circular neighborhoods is introduced in [9]. Recently, a learning 2D co-occurrence LBP is described to attain scale invariance for image recognition [10]. Deep architectures have been developed underlying the LBP for textural feature extraction for face recognition [37]. Empirical model with local binary convolution layers is explored [38]. Weighted-LBP emphasizes more importance on regions which are more influenced by aging effects [39]. Multi-scale LBP and SIFT descriptors are used for multi-feature discriminant analysis in [40]. The VGG-Face model is used for extracting the features for face recognition [41]. A journey of LBP since the past two decades is sketched in [33]. With a brief study, this paper explores a combination of deep features using CNN and texture features using LBP for classifying images with diverse categories.

3 Proposed Method: Deep Networks fused with Textures

Proposed DNT is a two-stream deep model (Fig. 1). Firstly, it emphasizes the features via patches and LSTM. Then, it combines multiple LBP. Lastly, both paths are fused.

3.1 Convolutional Feature Representation

An input color image with its class-label $I_l \in \mathbb{R}^{h \times w \times 3}$ is fed into a base CNN, such as DenseNet-121, etc. A CNN, say N extracts high-level feature map $F \in \mathbb{R}^{h \times w \times c}$ where h , w , and c denote the height, width, and channels, respectively. Simply, we denote $N(I_l, \theta) \rightarrow F$ to compute deep features, where image I_l is provided with its class-label l , and θ represents the learning parameters of N . The feature map F from the last convolutional layer of base N is extracted to develop the proposed model by including other functional modules.

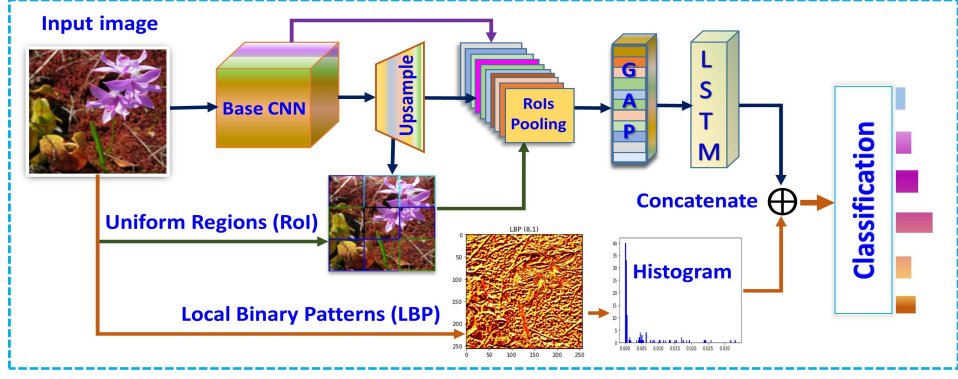


Fig. 1: Proposed method (DNT) fuses deep features and texture descriptors using local binary patterns (LBP) for fine-grained image classification.

3.2 Patch Encoding

The region proposals (D) are generated as non-overlapped uniform (same size) patches from I_l . The resulting number of regions is $e = (h \times w)/a^2$, where $a \times a$ is spatial size of a rectangular patch d . A set $D = \{d_1, d_2, \dots, d_e | I_l\}$ of e patches are pooled from feature map F which is spatially upsampled to $h' \times w' \times c$ size prior to pooling. The patches represent fine-details and local contexts which are important for subtle discrimination in FGIC. The bilinear pooling is applied to compute features from every patch of size $h_1 \times w_1 \times c$. Next, the global average pooling (GAP) is applied to summarize the mean features of D . It downsamples the spatial dimension at patch-level to $1 \times 1 \times c$. The resulting feature map is F_1 . To learn effectiveness of patches, a single layer fully-gated LSTM [42] is applied to learn long-term dependencies via the hidden states. The encoded feature vector is denoted as $F_2 \in \mathbb{R}^{v \times 1}$, defined in (Eq. 1).

$$F = N(I_l, \theta); \quad F_1 = N(D, GAP(F), \theta_1); \quad F_2 = N(D, LSTM(F_1), \theta_2) \quad (1)$$

3.3 Textures Representation using Local Binary Patterns

The local binary pattern (LBP) is a monotonic grayscale-invariant local descriptor which computes spatial textures. The histogram of LBP labels is considered as a feature vector. Here, the uniform value of $LBP_{P,R}$ is extracted as texture descriptor at global image-level. P defines total number of sampled neighbors, and R represents the radius of circular neighborhood.

$$LBP_{P,R} = \sum_{i=0}^{P-1} q(p_i - p_c) \cdot 2^i; \quad q(p_i - p_c) = \begin{cases} 1, & \text{if } (p_i - p_c) \geq 0 \\ 0, & \text{otherwise} \end{cases} \quad (2)$$

Here, p_c denotes grayscale value of center-pixel of a local window, and p_i represents value of corresponding neighbor pixel of p_c , and $q(\cdot)$ is an indicator function. The histograms of multiple neighborhoods are combined to improve the effectiveness of texture patterns. The



Fig. 2: Top-row: LBP of various neighborhoods (P, R): (8,1), (8,2), (16,1), and (16,2). Bottom-row: Random erasing data augmentation on flower and celebrity-face images.

descriptor F_3 is defined as

$$F_3 = \left\| \begin{array}{c} P, R \\ i=j=1 \end{array} \right\| LBP(I)_{P_i, R_j}; F_{final} = N(F_2 \left\| F_3, \theta_f \right.); \bar{l} = softmax(F_{final}); \bar{l} \in \mathbb{R}^{Y \times 1} \quad (3)$$

where, $\left\| \right\|$ denotes concatenation operator. The neighborhood spatial structures of $P = 8, 16$ and $R = 1, 2$ combinations are considered, shown in top-row of Fig. 2. The dimension of combined image-level texture vector is $4 \times 256 = 1024$. However, other higher values can also be computed according to Eq. 2-3.

3.3.1 Fusion

Finally, F_2 and F_3 are concatenated to produce a mixed feature vector F_{final} which is fed to a *softmax* layer for generating an output probability vector implying each predicted class-label \bar{l} corresponds to actual-label $l \in Y$ from a set of classes Y .

3.4 Random Region Erasing Image Augmentation

Several image augmentation methods are used *e.g.*, translation, rotation, scaling, random erasing [6], [7], etc. Here, random erasing at global image-level is applied along with general data augmentations. It randomly selects a rectangular region I_E in I , and erases pixels inside I_E with random values within $[0, 255]$. The height and width of I_E are randomly chosen on-the-fly within $[0.2, 0.8]$ scale, and pixels are erased with value 127. Examples are shown in the bottom-row of Fig. 2.



Fig. 3: Dataset samples are shown column-wise: human faces of FG-Net and celebrity, hand shape, and ISIC skin lesions.

4 Experimental Results and Discussion

Firstly, the datasets are summarised, followed by the implementation details. The performance evaluation and comparison with state-of-the-arts are discussed next.

4.1 Dataset Summary

Proposed DNT is evaluated on eight datasets representing the human faces, hand-shapes, food dishes, flowers, marine-lives, and skin lesions. A well-known age-invariant human face dataset, FG-Net contains 1002 images of 82 persons with ages from 0 to 69 years [12]. A touch-less hand database, called REgim Sfax Tunisia (REST), is mainly used for palmprint (biometric) recognition using local texture and shape descriptors [13]. A subset of REST dataset containing at least 5 left-hand images (2 images for testing and remaining 3 or more for training per class) of 179 individuals each is used in our work. The datasets comprised with 80 Indian dishes [15] and 50 Thailand dishes [16] are tested. Remaining 4 datasets *i.e.*, the celebrity faces ¹, flowers ², marine animals ³, and skin lesions ⁴ are collected from the Kaggle repository. The images are randomly divided into decent train-test sets, detailed in Table 1. Dataset samples are shown in Fig. 3-4. The top-1 accuracy (%) is evaluated for assessment and the model parameters are estimated in millions (M).

4.2 Implementation

The DenseNet-121, DenseNet-201, ResNet-50, and MobileNet-v2 backbone CNNs are used for deep feature extraction, and fine-tuned on the target datasets. Pre-trained ImageNet weights are used to initialize base CNNs with input image-size 256×256 . Random region

¹<https://www.kaggle.com/datasets/vishesh1412/celebrity-face-image-dataset>

²<https://www.kaggle.com/datasets/alexmaev/flowers-recognition>

³<https://www.kaggle.com/datasets/vencerlanz09/sea-animals-image-dataset>

⁴<https://www.kaggle.com/datasets/nodoubtome/skin-cancer9-clasesisisic>



Fig. 4: Dataset samples are shown column-wise: food-dishes of India and Thailand, natural objects representing flower and marine-lives.

Table 1: Dataset summary and test results using 3×3 patches and 256×256 LBP

Dataset	Class	Train	Test	DenseNet121	ResNet50	DenseNet201	MobileNetv2
FG-Net	82	827	175	52.38	48.80	57.73	52.38
Celebrity	17	1190	510	94.24	89.28	95.04	92.85
Indian Food	80	2400	1600	72.18	68.87	73.31	69.62
Thai Food	50	14172	1600	92.31	90.18	92.50	89.93
Flower	6	2972	1400	96.85	95.78	96.71	96.07
Sea-life	18	5823	3636	90.36	89.10	91.05	90.09
REST-Left Hand	179	616	358	79.73	81.25	80.96	77.27
ISIC Skin Cancer	7	1491	675	78.86	77.23	79.45	73.06
Model Parameters (Millions)				10.2	29.0	23.5	6.1

erasing, rotation (± 25 degrees), scaling (± 0.25), and cropping 224×224 image-size are followed for data augmentation. The output feature map (e.g., $7 \times 7 \times c$) is upsampled to $48 \times 48 \times c$ for pooling of 4×4 patches, and the value of output channels (c) varies according to CNN architectures, e.g., $c = 1024$ for DenseNet-121. Uniform patch-size is 12×12 pixels to generate 16 patches. The feature size of LSTM’s hidden layers is 1024, and concatenated with LBP of same size. The final feature vector $c = 2048$ is fed to the softmax layer for classification. Batch normalization and drop-out rate is 0.2 is applied to ease over-fitting. The Stochastic Gradient Descent (SGD) optimizer is used to optimize the categorical cross-entropy loss with an initial learning rate of 10^{-3} and divided by 10 after 100 epochs. The DNT model is trained for 200 epochs with a mini-batch size of 8 using 8 GB Tesla M10 GPU, and scripted in Python.

4.3 Result Analysis and Performance Comparison

The test results with 3×3 patches and two LBP structures *i.e.*, (8, 1) and (8, 2) with a total 512 textures are given in Table 1. The feature size of LSTM’s hidden unit is 512, and after concatenating with histograms of LBP, size of final feature map is 1024. The last-row estimates the parameters (Millions) of various models. The accuracy (%) is very decent, except age-invariant face recognition (AIFR) *i.e.*, FG-Net. Many existing methods have experimented on FG-Net dataset for AIFR by following leave-one-person out strategy [41], [43]. In our set-up, FG-Net test-set includes at least one unseen image per person by splitting 1002 samples into train-test (83:17) sets. Here, we have tested this challenging dataset for FGIC rather than AIFR. Hence, DNT is not directly comparable with existing methods. However, DNT attains better results (Table 1 and Table 3) than NTCA (48.96%) [44], and other works on AIFR [11].

The REST dataset [13] is primarily tested for palmprint based biometric identification using traditional textures and more recently using CNNs. In this work, we have tested the left-hand images of REST dataset for classification using full hand-shapes and its class-labels only, *i.e.*, without determining any region of interests for palmprint, or additional pre-processing stage. The proposed DNT has achieved 85.79% top-1 accuracy using DenseNet-201. The precision is 90.0% and recall is 86.0%. On the contrary, the SIFT descriptors [13] reported 80.83% palmprint identification success with the samples of 150 persons. Though, our DNT is not directly comparable with this existing work, yet, the gain of our method is significant on this dataset. The ISIC 2017 dataset comprising with 2000 lesion images are classified into 3 categories, namely Melanoma, Seborrheic keratosis and Nevu in [29]. The classification accuracy is 85.7% using Lesion Indexing Network (LIN). However, our method is not directly comparable with LIN [29]. Our DNT has classified 7 skin diseases namely actinic keratosis, basal cell carcinoma, melanoma, nevus, pigmented benign keratosis, squamous cell carcinoma, and vascular lesion. The accuracy is 81.10% using DenseNet-201 backbone. The confusion matrices are shown in Fig. 5, representing the performance of DNT using ResNet-50 and DenseNet-201 base CNNs.

FoodNet presents classification of 50 Indian food-dishes [15], and achieves 73.50% accuracy using an ensemble method. It consists 100 images per class and 80% images per class are used for training. We have used similar 80 dishes with 50 images per class, following 60:40 train-test ratio. DNT achieves 80.75% and 74.75% accuracy using DenseNet-201 and ResNet-50, respectively (Table 3). We have tested on ThaiFood-50 [16], and the accuracy is 80.42%. In [45], the accuracy is 83.07% using ResNet-50. On the contrary, DNT attains 95.18% using DenseNet-201, and 91.93% by ResNet-50 (Table 3).

The performance on other datasets are also high. However, to the best of our knowledge, no significant results have been reported on dataset, like sea-life. We have reported the results in the context of FGIC on these datasets for further research.

The overall classification performances of various CNNs using 3×3 patches and 2×256 LBP on Indian food dishes and celebrity faces are shown in Fig. 6. It is evident that accuracy improvement is very small after 100 epochs. ResNet-50 and Xception are comparatively heavier models than the DenseNet family regarding the model parameters. Whereas, MobileNet-v2 is a lightweight model, yet, very efficient for FGIC.

Next, experiments on Indian food and flower show accuracy gain using 4×4 patches while other components are unaltered. This test is comprised with 16 patches, 512 LBP and 512 LSTM features. The results imply more patches improve accuracy (Table 2).

Table 2: Performance of DNT using 16 patches and 512 LBP

Dataset	DenseNet-121	ResNet-50	DenseNet-201	MobileNet-v2
Flower	97.10	94.78	96.50	95.71
Indian Food	72.13	71.43	76.06	72.94
Param (M)	10.3	28.8	23.3	6.0

Table 3: Performance of DNT using 16 patches and 1024 LBP

Dataset	DenseNet-121	ResNet-50	DenseNet-201	MobileNet-v2
FG-Net	54.74	49.40	55.95	53.57
Celebrity	95.43	92.06	95.83	90.87
Indian Food	78.18	74.75	80.75	76.31
Thai Food	94.00	91.93	95.18	92.75
Flower	97.50	97.14	98.00	97.21
Sea-life	92.50	92.51	94.51	92.34
REST-Left Hand	83.52	83.23	85.79	80.14
ISIC Skin Cancer	80.50	78.42	81.10	77.52
Param (M)	15.8	36.5	30.8	12.1

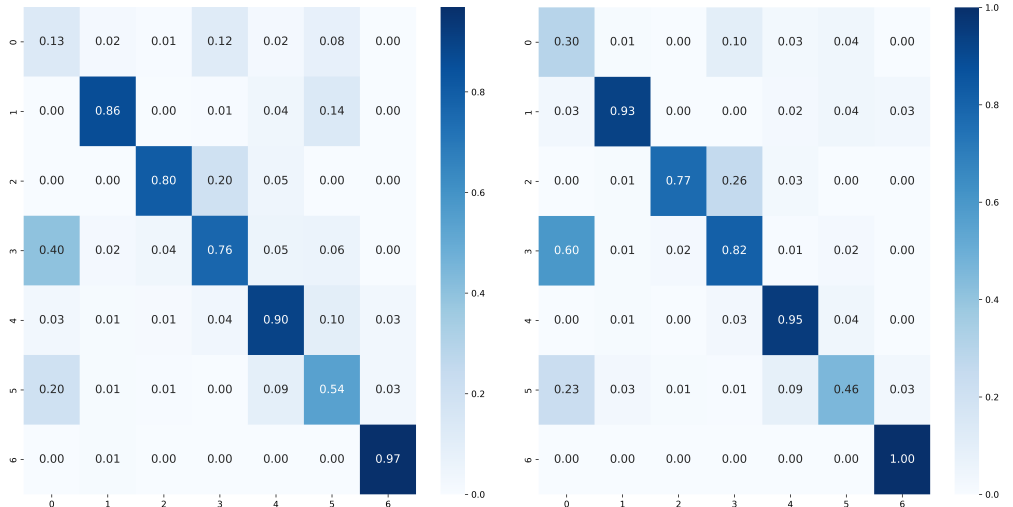


Fig. 5: Confusion matrix on ISIC skin cancer dataset using DNT with 4×4 patches and 2×1024 LBP based on ResNet-50 (left) and DenseNet-201 (right) backbone CNNs.

We have increased the number of LSTM’s hidden states and number of patches. This test is carried out with the fused features of 1024 textures (LBP), and 1024 LSTM units encoded from 16 patches. The results are reported in Table 3. Clearly, DenseNet-201 performs the best among four base CNNs, while other backbones produce satisfactory results.

The significance of major components of DNT are tested, and the results are given in Table 4. Particularly, the benefits of random erasing over general image augmentation, number of patches, textures (LBP), LSTM, and their further increment in the feature space are

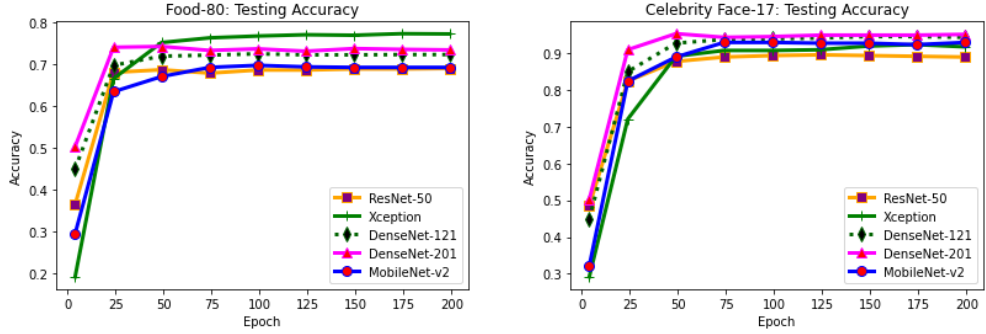


Fig. 6: Test accuracy of various CNNs using 3×3 patches and 2×256 LBP on Indian food-80 and celebrity faces datasets.

Table 4: Ablation study on proposed DNT using DenseNet-121 (DN-121)

DenseNet-121 (DN-121) base CNN with key modules	Indian Food	Sea-life	Param
DN-121 + common image augmentation	63.37	86.24	7.0
DN-121 + common + random erasing image augment	67.25	88.43	7.0
DNT (DN-121) with 9 patches, and LBP (addition)	71.49	89.23	10.2
DNT (DN-121) with 16 patches, and without LBP	74.56	90.28	15.5
DNT (DN-121) with 16 patches, and LBP (concatenation)	78.18	92.50	15.5

investigated for performance improvement on two datasets using DenseNet-121 (DN-121). The ablative results justify the usefulness of essential components of the proposed DNT.

5 Conclusion

In this paper, we have presented a new work on image classification by fusing the deep features with local textures at image-level. The performance is evaluated using four base CNNs on eight diverse FGIC datasets. We have achieved better results on these datasets compared to mentioned existing works. In addition with conventional image augmentation, random region erasing data augmentation improves the accuracy. The ablation study reflects the usefulness of important components. In future, we plan to develop a new model to improve the performance further and explore other fusion strategies for wider applicability on diverse datasets.

Acknowledgement

We thank to the Reviewers to improve this paper. We thank to the repositories for the datasets used in this work. We are thankful to BITS Pilani, Pilani Campus, Rajasthan, India, for providing necessary infrastructure and Research Initiation Grant to carry out this work.

References

- [1] Wei, X.-S., Wu, J., Cui, Q.: Deep learning for fine-grained image analysis: A survey. arXiv preprint arXiv:1907.03069 (2019)
- [2] Liu, H., Li, J., Li, D., See, J., Lin, W.: Learning scale-consistent attention part network for fine-grained image recognition. *IEEE Transactions on Multimedia* **24**, 2902–2913 (2022)
- [3] Bera, A., Wharton, Z., Liu, Y., Bessis, N., Behera, A.: Attend and guide (ag-net): A keypoints-driven attention-based deep network for image recognition. *IEEE Transactions on Image Processing* **30**, 3691–3704 (2021)
- [4] Ge, W., Lin, X., Yu, Y.: Weakly supervised complementary parts models for fine-grained image classification from the bottom up. In: Proc. IEEE Conf. Comput. Vis. Pattern Recognit., pp. 3034–3043 (2019)
- [5] Behera, A., Wharton, Z., Hewage, P., Bera, A.: Context-aware attentional pooling (cap) for fine-grained visual classification. In Proc. 35th AAAI Conference on Artificial Intelligence, 929–937 (2021)
- [6] Zhong, Z., Zheng, L., Kang, G., Li, S., Yang, Y.: Random erasing data augmentation. In: Proc. AAAI Conf. on Artificial Intelligence, vol. 34, pp. 13001–13008 (2020)
- [7] Bera, A., Nasipuri, M., Krejcar, O., Bhattacharjee, D.: Fine-grained sports, yoga, and dance postures recognition: A benchmark analysis. *IEEE Transactions on Instrumentation and Measurement* **72**, 1–13 (2023)
- [8] Liu, M., Zhang, C., Bai, H., Zhang, R., Zhao, Y.: Cross-part learning for fine-grained image classification. *IEEE Transactions on Image Processing* **31**, 748–758 (2022)
- [9] Ojala, T., Pietikainen, M., Maenpaa, T.: Multiresolution gray-scale and rotation invariant texture classification with local binary patterns. *IEEE Transactions on Pattern Analysis and Machine Intelligence* **24**(7), 971–987 (2002)
- [10] Bi, X., Yuan, Y., Xiao, B., Li, W., Gao, X.: 2d-lcolbp: A learning two-dimensional co-occurrence local binary pattern for image recognition. *IEEE Trans. Image Processing* **30**, 7228–7240 (2021)
- [11] Panis, G., Lanitis, A., Tsapatsoulis, N., Cootes, T.F.: Overview of research on facial ageing using the fg-net ageing database. *IET Biometrics* **5**(2), 37–46 (2016)
- [12] Panis, G., Lanitis, A.: An overview of research activities in facial age estimation using the fg-net aging database. In: European Conf. Computer Vision, pp. 737–750 (2014)
- [13] Charfi, N., Trichili, H., Alimi, A.M., Solaiman, B.: Local invariant representation for multi-instance toucheless palmprint identification. In: 2016 IEEE International Conference on Systems, Man, and Cybernetics (SMC), pp. 003522–003527 (2016)

- [14] Olayah, F., Senan, E.M., Ahmed, I.A., Awaji, B.: Ai techniques of dermoscopy image analysis for the early detection of skin lesions based on combined cnn features. *Diagnostics* **13**(7), 1314 (2023)
- [15] Pandey, P., Deepthi, A., Mandal, B., Puhan, N.B.: Foodnet: Recognizing foods using ensemble of deep networks. *IEEE Signal Processing Letters* **24**(12), 1758–1762 (2017)
- [16] Termritthikun, C., Kanprachar, S.: Accuracy improvement of thai food image recognition using deep convolutional neural networks. In: 2017 International Electrical Engineering Congress (IEECON), pp. 1–4 (2017). IEEE
- [17] Bera, A., Bhattacharjee, D., Nasipuri, M.: Deep neural networks fused with textures for image classification. In: International Conference on Frontiers in Computing and Systems, pp. 103–111 (2022). Springer
- [18] Dosovitskiy, A., Beyer, L., Kolesnikov, A., Weissenborn, D., Zhai, X., Unterthiner, T., Dehghani, M., Minderer, M., Heigold, G., Gelly, S., et al.: An image is worth 16x16 words: Transformers for image recognition at scale. *arXiv preprint:2010.11929* (2020)
- [19] Tianskaew, U., Chunpongthong, P., Mettanant, V.: A food photography app with image recognition for thai food. In: 2018 Seventh ICT International Student Project Conference (ICT-ISPC), pp. 1–6 (2018). IEEE
- [20] Lim, C.H., Goh, K.M., Lim, L.L.: Explainable artificial intelligence in oriental food recognition using convolutional neural network. In: 2021 IEEE 11th International Conference on System Engineering and Technology (ICSET), pp. 218–223 (2021)
- [21] Arslan, B., Memiş, S., Sönmez, E.B., Batur, O.Z.: Fine-grained food classification methods on the uec food-100 database. *IEEE Trans. Artificial Intelligence* **3**(2), 238–243 (2021)
- [22] Min, W., Jiang, S., Liu, L., Rui, Y., Jain, R.: A survey on food computing. *ACM Computing Surveys (CSUR)* **52**(5), 1–36 (2019)
- [23] Aguilar, E., Nagarajan, B., Radeva, P.: Uncertainty-aware selecting for an ensemble of deep food recognition models. *Computers in Biology and Medicine* **146**, 105645 (2022)
- [24] Xu, S., Zhang, M., Song, W., Mei, H., He, Q., Liotta, A.: A systematic review and analysis of deep learning-based underwater object detection. *Neurocomputing* (2023)
- [25] Wang, N., Chen, T., Liu, S., Wang, R., Karimi, H.R., Lin, Y.: Deep learning-based visual detection of marine organisms: A survey. *Neurocomputing* **532**, 1–32 (2023)
- [26] Hasan, M.K., Ahamad, M.A., Yap, C.H., Yang, G.: A survey, review, and future trends of skin lesion segmentation and classification. *Computers in Biology and Medicine*, 106624 (2023)
- [27] Codella, N.C., Gutman, D., Celebi, M.E., Helba, B., Marchetti, M.A., Dusza, S.W.,

- Kalloo, A., Liopyris, K., Mishra, N., Kittler, H., *et al.*: Skin lesion analysis toward melanoma detection: A challenge at the 2017 international symposium on biomedical imaging (isbi), hosted by the international skin imaging collaboration (isic). In: 2018 IEEE 15th International Symposium on Biomedical Imaging, pp. 168–172 (2018)
- [28] Cassidy, B., Kendrick, C., Brodzicki, A., Jaworek-Korjakowska, J., Yap, M.H.: Analysis of the isic image datasets: Usage, benchmarks and recommendations. *Medical image analysis* **75**, 102305 (2022)
- [29] Li, Y., Shen, L.: Skin lesion analysis towards melanoma detection using deep learning network. *Sensors* **18**(2), 556 (2018)
- [30] Liu, X., Jia, Z., Hou, X., Fu, M., Ma, L., Sun, Q.: Real-time marine animal images classification by embedded system based on mobilenet and transfer learning. In: OCEANS 2019-Marseille, pp. 1–5 (2019). IEEE
- [31] Pedersen, M., Bruslund Haurum, J., Gade, R., Moeslund, T.B.: Detection of marine animals in a new underwater dataset with varying visibility. In: Proc. of the IEEE/CVF Conference on Computer Vision and Pattern Recognition Workshops, pp. 18–26 (2019)
- [32] Bera, A., Bhattacharjee, D.: Human identification using selected features from finger geometric profiles. *IEEE Trans. Systems, Man, and Cybernetics: Systems* **50**(3), 747–761 (2020)
- [33] Pietikäinen, M., Zhao, G.: Two decades of local binary patterns: A survey, pp. 175–210. Elsevier (2015)
- [34] Bera, A., Bhattacharjee, D., Nasipuri, M.: Person recognition using alternative hand geometry. *International Journal of Biometrics* **6**(3), 231–247 (2014)
- [35] Barata, C., Ruela, M., Francisco, M., Mendonça, T., Marques, J.S.: Two systems for the detection of melanomas in dermoscopy images using texture and color features. *IEEE systems Journal* **8**(3), 965–979 (2013)
- [36] Bera, A., Bhattacharjee, D., Shum, H.P.: Two-stage human verification using hand-captcha and anti-spoofed finger biometrics with feature selection. *Expert Systems with Applications* **171**, 114583 (2021)
- [37] Xi, M., Chen, L., Polajnar, D., Tong, W.: Local binary pattern network: A deep learning approach for face recognition. In: 2016 IEEE International Conf. Image Processing (ICIP), pp. 3224–3228 (2016). IEEE
- [38] Juefei-Xu, F., Naresh Boddeti, V., Savvides, M.: Local binary convolutional neural networks. In: Proc. IEEE Computer Vision and Pattern Recognition, pp. 19–28 (2017)
- [39] Zhou, H., Lam, K.-M.: Age-invariant face recognition based on identity inference from appearance age. *Pattern recognition* **76**, 191–202 (2018)

- [40] Li, Z., Park, U., Jain, A.K.: A discriminative model for age invariant face recognition. *IEEE Trans. Information Forensics and Security* **6**(3), 1028–1037 (2011)
- [41] Moustafa, A.A., Elnakib, A., Areed, N.F.: Age-invariant face recognition based on deep features analysis. *Signal, Image and Video Processing* **14**(5), 1027–1034 (2020)
- [42] Hochreiter, S., Schmidhuber, J.: Long short-term memory. *Neural computation* **9**(8), 1735–1780 (1997)
- [43] Zhao, J., Yan, S., Feng, J.: Towards age-invariant face recognition. *IEEE Transactions on Pattern Analysis and Machine Intelligence* **44**(1), 474–487 (2022)
- [44] Bouchaffra, D.: Nonlinear topological component analysis: application to age-invariant face recognition. *IEEE Trans. Neural Networks and Learning Systems* **26**(7), 1375–1387 (2014)
- [45] Termritthikun, C., Kanprachar, S.: Nu-resnet: Deep residual networks for thai food image recognition. *Journal of Telecommunication, Electronic and Computer Engineering (JTEC)* **10**(1-4), 29–33 (2018)